

Photochemical & Photobiological Sciences

Accepted Manuscript



This is an *Accepted Manuscript*, which has been through the Royal Society of Chemistry peer review process and has been accepted for publication.

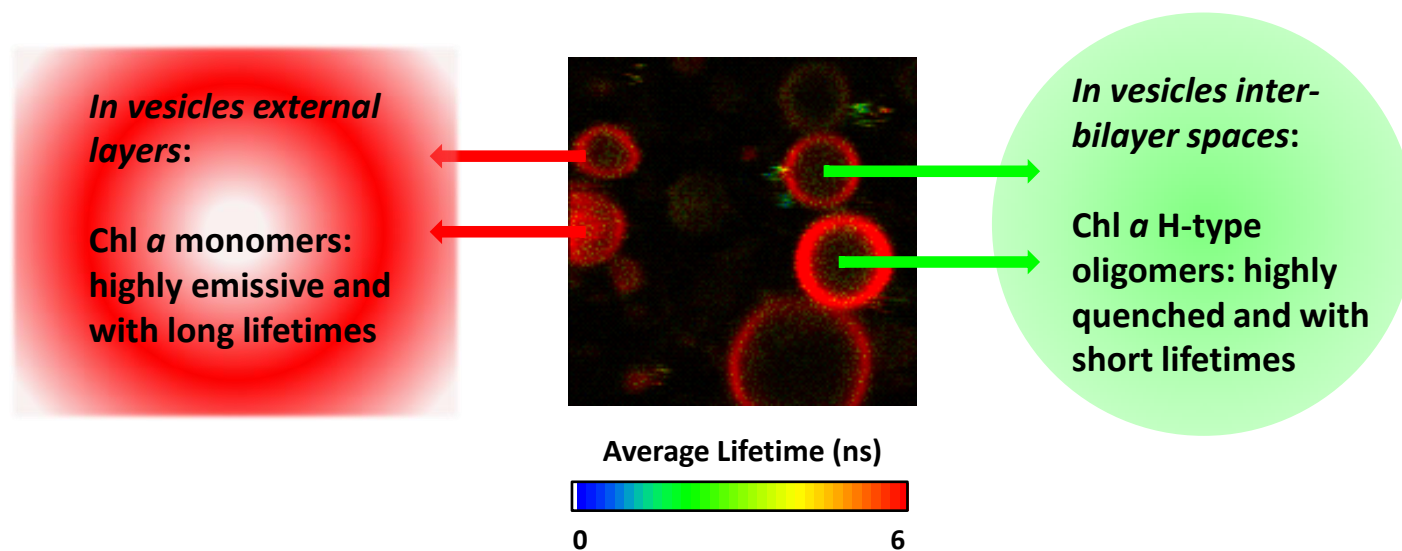
Accepted Manuscripts are published online shortly after acceptance, before technical editing, formatting and proof reading. Using this free service, authors can make their results available to the community, in citable form, before we publish the edited article. We will replace this *Accepted Manuscript* with the edited and formatted *Advance Article* as soon as it is available.

You can find more information about *Accepted Manuscripts* in the [Information for Authors](#).

Please note that technical editing may introduce minor changes to the text and/or graphics, which may alter content. The journal's standard [Terms & Conditions](#) and the [Ethical guidelines](#) still apply. In no event shall the Royal Society of Chemistry be held responsible for any errors or omissions in this *Accepted Manuscript* or any consequences arising from the use of any information it contains.

Graphical Abstract

FLIM image of Chl *a* in pure DMPC liposomes (*at the centre*) ; and most found Chl *a* species: Chl *a* monomers in vesicles outer monolayers (*left*); Chl *a* H-type dimers/aggregates in vesicles inter-bilayer spaces (*right*).



Aggregation/Disaggregation of Chlorophyll *a* in Model Phospholipid–Detergent Vesicles and Micelles[▼]

Cite this: DOI: 10.1039/x0xx00000x

Raquel F. Correia,^{a,b} M. Isabel Viseu,^{*,a} Suzana M. Andrade^aReceived 00th January 2012,
Accepted 00th January 2012

DOI: 10.1039/x0xx00000x

www.rsc.org/

The photosynthetic pigments of higher plants exist in complex oligomeric states, which are difficult to study in vivo. To investigate aggregation processes of chlorophyll *a* (Chl *a*), we used an in vitro reconstitution procedure, with this pigment incorporated in liposomes of 1,2-dimyristoyl-*sn*-glycero-3-phosphocholine (DMPC), micelles and pre-micelle media of the detergent *n*-dodecyltrimethylammonium chloride (DTAC), and mixed, spontaneous, DMPC–DTAC vesicles and micelles. Chl *a* oligomers were characterized by UV–visible absorption, steady-state and time-resolved fluorescence, and fluorescence lifetime imaging microscopy. Equivalent diameters of the colloidal structures were obtained by fluorescence correlation spectroscopy. In DMPC liposomes and DMPC–DTAC vesicles and micelles, three fluorescence lifetimes indicated the coexistence of Chl *a* monomers (≈ 5 ns) and oligomers (≈ 1 – 2 to ≈ 0.1 ns). The increase in DTAC amount, in the mixed system, induces a progressive solubilization of DMPC liposomes (from vesicles to micelles) and simultaneous disruption of Chl *a* aggregates: in pure DTAC micelles, mostly monomers were found. The present work aims to a better understanding of chlorophyll–chlorophyll (Chl–Chl), Chl–lipid, and Chl–detergent interactions, in spontaneous colloidal micro- and nanostructures.

Introduction

The interaction of chlorophyll *a* (Chl *a*)^{*} and other porphyrinoids with DMPC liposomes has received an extensive attention in the important area of photodynamic therapy, PDT [1–3], an anticancer treatment in which a photosensitizing drug accumulated in tumor tissues is activated by light, leading to death of the malignant cells. Chl *a* and its derivatives have shown useful characteristics for PDT, mainly strong absorption, allowing light penetration into tissues, and high phototoxicity to tumor cells with no toxicity to healthy ones [4,5]. Associated to proper carriers, such as liposomes or other lipid assemblies, Chl *a* and derivatives can be potential PDT photosensitizers.

media; 4- Fluorescence lifetimes of Chlorophyll *a* in DMPC–DTAC media; 5- FLIM images of Chlorophyll *a* in DTAC pre-micelle media; 6- FCS parameters for Chlorophyll *a* in DMPC–DTAC media. This material will be published online in DOI: 10.1039/x0xx00000x

*Abbreviations and symbols:

Chl (*a*), Chlorophyll (*a*);
CMC, Critical micelle concentration;
DMPC, 1,2-Dimyristoyl-*sn*-glycero-3-phosphocholine;
DTAC, *n*-Dodecyltrimethylammonium chloride;
D, Detergent (DTAC);
L, Lipid (DMPC);
D:L, Detergent to lipid molar ratio;
DLS, Dynamic light scattering;
FCS, Fluorescence Correlation Spectroscopy;
FLIM, Fluorescence Lifetime Imaging Microscopy;
TCSPC, Time-correlated single-photon counting;
MLV(s), Multilamellar vesicle(s);
ULV(s), Unilamellar vesicle(s);
Disk(s), Discoidal micelle(s);
Thread(s), Threadlike micelle(s);
D, Diffusion coefficient (for spherical particles in diluted media);
 Φ , Hydrodynamic diameter;
 Φ_e , Neutral-sphere-equivalent hydrodynamic diameter;
 τ , Fluorescence lifetime;
 τ_D , (Average) diffusion time.

* Corresponding author. E-mail: isabelviseu@tecnico.ulisboa.pt^a Centro de Química Estrutural, Instituto Superior Técnico, Universidade de Lisboa, 1049-001 Lisboa, Portugal.^b Current address: Dipartimento di Scienze Chimiche e Geologiche, University of Cagliari, Cittadella di Monserrato, I-09042 Monserrato–Cagliari, Italy.

▼ Electronic supplementary information (ESI) available: 1- Turbidity correction of electronic absorption spectra of Chlorophyll *a* in DMPC–DTAC media; 2- Parameters of electronic absorption spectra of Chlorophyll *a* in DMPC–DTAC media; 3- Steady-state fluorescence of Chlorophyll *a* in DTAC

Chl *a* is the main pigment of the photosynthetic process of higher plants and algae. These organisms capture directly the sun light and use it as a source of energy to convert water into oxygen. Light is captured by a sophisticated system of several hundred Chls and accessory pigments, which act as antennae to absorb the incident quantum flux and to transfer it to special Chls in the reaction centres. The characteristic functions of Chl *a* as energy collector, in the antenna, and primary electron carrier, in the reaction center, act cooperatively, and strongly depend on its molecular organization/aggregation in the lipid matrix of thylakoid membranes.

Photosynthetic organisms employ transmembrane pigment–protein light-harvesting complexes, LHCI and LHCII (of PSI and PSII, respectively), the latter being the most abundant in green plants. It is well known that the Chl aggregation and consequent decrease of its fluorescence yield can be reversed by detergent addition. The 2-D structure of the lipidic membrane seems to be important to regulate the LHCII organization and function, and thus the LHCII ability to undergo light-induced reversible structural changes. Furthermore, the structural flexibility of the LHCII macro-aggregates is strongly influenced by the content and nature of the lipid [6,7].

Based on these aspects, model membrane systems were used in this work to study the influence of the detergent/lipid composition on the Chl *a* aggregation/disaggregation, to obtain a better understanding of the role of Chl in photosynthesis.

Even though the major part of Chl *a* in photosynthetic membranes is complexed with proteins in the LHCI and LHCII [8], we do not model herein Chl–protein interactions. A small fraction of Chl *a* (2–3%) remains free in the living membranes [9–11], which is less than 1% of the total thylakoid lipid content [12]. According to this, the Chl *a* content in our *in vitro* samples is below 0.2% v/v (see the Samples preparation subsection).

Chl *a* is in complex oligomeric states in the living photosynthetic organisms. Aggregation of Chl has been investigated for decades, since Shipman et al. proposed its model of the Chl *a* special pair in 1976 [13]. Katz et al. (1978, 1979, 1991) [14–16] and Scherz et al. (1991) [17] also made relevant studies on this area, proposing model schemes for the pigment dimers and oligomers in aqueous solvents.

Usual approaches to study Chl *a* aggregation have been to incorporate the pigment into simplified *in vitro* models, such as mixtures of organic solvents with water [18,19] and surfactant (phospholipid, detergent) assemblies [20–24]. Being able to compartmentalize Chl *a* in their hydrophobic/hydrophilic microenvironment, surfactant assemblies (liposomes, micelles) have often been used as models of thylakoid membranes. However, these latter systems have been less investigated than solvent mixtures.

The major lipids existing in thylakoid membranes are *zwitterionic* lipids, namely phosphocholines [25,26]. On the other hand, *cationic* detergents are commonly used to reconstruct the state of Chl *a* dissolved in the lipid phase of thylakoid membranes [27].

In previous work, the spontaneous nano- and micro-colloidal structures formed in DMPC liposome solubilization by the cationic detergent DTAC, at varying detergent to lipid (D:L) molar ratios,

were characterized: A multi-step transition, from multilamellar (MLVs) to unilamellar vesicles (ULVs), to ruptured vesicles, curved bilayer fragments, and bicelles (or disks), and, finally, to spherical and threadlike micelles, was found [28,29].

Taking advantage of the previous detailed characterization of the DTAC–DMPC colloidal structures, in the present work we use Chl *a* as a sensor of these structures to deeply investigate their size and morphology. On the other hand, the spectral behavior and time-resolved fluorescence of the probe in the colloidal structures are used to investigate how these structures affect the known tendency of Chl *a* to self-assemble.

Fluorescence lifetime imaging microscopy (FLIM) provides not only the image contrast but also fluorescence decay times, which depend on the fluorophore photophysical behavior and the physico-chemical properties of the surrounding medium [30,31]. Therefore, FLIM images of Chl *a* inserted in giant colloidal structures, vesicles and cylindrical (threadlike) micelles, gave the colloids morphology, as well as mean lifetimes of Chl *a* monomers and oligomers. Equivalent diameters of the colloidal nanostructures containing Chl *a*, obtained by fluorescence correlation spectroscopy (FCS), were compared with published DLS data [29].

Experimental

Materials

Chlorophyll *a*, extracted from spinach and substantially free from chlorophyll *b*, was purchased from Sigma. Chl *a* stock solutions were prepared in diethyl ether (Sigma-Aldrich, >99.8% pure) and stored at ≈ 7 °C, protected from light. The samples purity and concentration were routinely checked by UV–visible absorption spectroscopy. DMPC (> 99% pure) was purchased from Avanti Polar Lipids, USA, and DTAC (> 98% pure) from TCI Europe, Belgium. Chloroform ($\approx 99.8\%$ pure), used for lipid and lipid–detergent dissolution, was obtained from Sigma–Aldrich. Bi-distilled water was purified with the Millipore Milli-Q system. All other substances were used without further purification.

Samples preparation

A small volume (< 0.2% v/v) of a Chl *a* stock solution in diethyl ether was injected into a concentrated DTAC micelle solution. DTAC has a CMC of 22.0–22.5 mM, at 25 °C [32]. After equilibration for 30 minutes at room temperature (24–25 °C), Millipore water was added to produce the required micelle or premicelle media. Pure DMPC vesicles, with a final lipid concentration of 0.75 mM, and lipid–detergent vesicles and micelles, with the same final lipid concentration and different detergent:lipid (D:L) total molar ratios, were prepared as described before [28,29], without sonication or extrusion to obtain only *spontaneous structures*. After 2 hours incubation in a water bath at 40 °C, samples stayed at room temperature for 15 minutes before injection of adequate volumes (< 0.2% v/v) of the stock solution of Chl *a* in diethyl ether.

The D:L order increases from pure DMPC ($D = 0$, or $D:L = 0$) to pure DTAC micelles or premicelle media ($L = 0$, or $D:L = \infty$). In absorption and emission spectra, the order of curves corresponds to a D:L decrease. However, emission lifetimes, FLIM images, and FCS data are presented in ascending order. Ascending or descending order was chosen to facilitate the discussion of the different types of results.

UV–Visible absorption and turbidity correction

Electronic absorption spectra were carried out on a Perkin–Elmer (Lambda 35) UV–visible absorption spectrometer, typically using the wavelength range of 250–850 nm and an optical path of 1 cm.

Background light scattering was corrected as explained before [33,34], by subtracting from each spectrum an empirical scattering function, s :

$$s(\lambda) = a + \frac{b}{\lambda^c} \quad (1)$$

In eq. 1, λ is the wavelength of the incident radiation, and a , b , and c are empirical parameters: a is a simple, usually negligible, background correction (e.g., for correcting slight differences in the cell position); b is a proportionality factor related to c ; and c depends strongly on the mean dimensions of the scattering particles as compared to the wavelength of the incident light. Briefly, the methodology consists of subtracting a power law fitted to the parts of the spectral baseline free from absorption bands. This power law is related to the dimensions, refractive index, size, and polydispersity of the scattering particles *through the parameter c*. For soft matter, c usually varies from 1–2 (very large particles) to 4 (very small particles) [35].

Steady-state fluorescence

Fluorescence emission spectra were carried out in a SPEX® Fluorolog spectrofluorimeter (HORIBA Jobin Yvon) in a FL3-11 configuration. Spectra were obtained with excitation at 638 nm, as an average of three measurements, and were corrected for the instrumental response by a function provided by the manufacturer.

Time-resolved fluorescence and fluorescence lifetime imaging microscopy (FLIM)

Fluorescence decays were acquired with a Microtime 200 equipment (Picoquant GmbH, Germany) using the time-correlated single-photon counting (TCSPC) technique. Excitation at 638 nm was obtained from a pulsed laser diode with a pulse width of 54 ps and a repetition rate of 20 MHz. A band-pass filter (695AF55 Omega optical), transmitting at 667–722 nm, eliminates most of the laser excitation scattered light and the solvent Raman scattered light in the photomultiplier tube (PicoQuant, PMA-182). Data were acquired in a PC equipped with a Timeharp 200 TCSPC board (PicoQuant) with 4096 channels and a time increment smaller than 40 ps. The laser

light was backscattered by the square base of a quartz fluorescence cuvette (optical path = 1 cm), and directed to the detection system to obtain the instrumental response function (IRF).

Lifetime data were analyzed with the software package Fluofit 4.2, a nonlinear least squares fitting program based on the Marquardt algorithm. The decays were fitted by a sum of exponential functions (eq. 2), using iterative deconvolution with the IRF:

$$F(t) = \sum_{i=1}^N a_i \exp\left(-\frac{t}{\tau_i}\right) \quad (2a)$$

In eq. 2a, a_i and τ_i are, respectively, the amplitude and time constant of the component i , and N is the number of exponential components. The goodness of the fit was evaluated by the usual statistical criteria (χ^2 parameter) and by visual inspection of the residuals distribution.

Intensity-weighted average lifetimes τ_{av} were obtained by the following equations [36]:

$$\tau_{av} = \frac{\sum_i^n a_i \tau_i^2}{\sum_i^n a_i \tau_i}; \quad \text{with: } \sum_i^n a_i = 1 \quad (2b;c)$$

FLIM measurements were performed with the same Microtime 200 equipment. Briefly, the 638 nm pulsed diode laser was focused by a water immersion objective (60 \times ; 1.2 NA) into the sample. Fluorescence was collected by the same objective, passed through the dichroic mirror and suitable band pass filter, and focused through a pinhole (50 μm , to reject out-of-focus light) onto a single-photon counting avalanche photodiode (Perkin–Elmer). The output signal was processed by the TimeHarp 200 TCSPC PC-board (PicoQuant), working in the special Time-Tagged Time-Resolved mode. The instrumental setup provides image resolution up to 50 nm per pixel; the final resolution is $\approx \lambda/2$.

A small drop (20 μL) of each aqueous solution was spread at 25 $^\circ\text{C}$ on the microscope coverslip, and directly imaged at 5–10 μm above its surface. Samples were not dried to prevent disruption (or morphology alteration) of colloidal structures; care was also taken to prevent solvent evaporation. Soon after deposition, no colloidal particles were found; about 1 hour later, micro-sized structures (≈ 1 –20 μm), such as giant vesicles (MLVs, ULVs) and threadlike micelles, which settled down in the drop solution, were captured.

Fluorescence correlation spectroscopy (FCS)

Chl a samples in the nanomolar range were investigated by FCS at 25 $^\circ\text{C}$, using the same Microtime 200 set-up from PicoQuant and the same excitation laser of 638 nm [37,38]. The focal area and detection volume were calibrated with the reference dye Atto655 in the carboxylic acid form (Atto-Tech GmbH, Germany), which has a diffusion coefficient of 426 $\mu\text{m}^2 \text{s}^{-1}$, in water, at 25 $^\circ\text{C}$.

At low intensity, the diffusion model assumes that the confocal volume can be approximated by a 3-dimensional Gaussian shape, eq. 3 [39], which was fitted to the experimental auto-correlation functions $G_D(\tau)$:

$$G_D(\tau) = \frac{1}{N} \left[1 + \frac{\tau}{\tau_D} \right]^{-1} \left[1 + \frac{\tau}{k^2 \tau_D} \right]^{-0.5} \quad (3)$$

N is the average number of molecules in the confocal volume, τ_D their average diffusion time in the same volume, and k the axial ratio (ratio of axial z_0 to radial ω_0 dimensions) of the confocal volume.

The diffusion time of a molecule, when modeled as a non-interacting, uncharged, spherical particle, is proportional to the square of the beam waist ω_0 at the focus of the laser beam [40,41], and allows the calculation of the translational diffusion coefficient D :

$$\tau_D = \frac{\omega_0^2}{4D} \quad (4)$$

Hydrodynamic diameters Φ were finally obtained by the Stokes–Einstein equation:

$$\Phi = \frac{k_B T}{3\pi\eta_0 D} \quad (5)$$

where k_B is the Boltzmann constant and η_0 the solvent viscosity at temperature T . Eq. 5 does not consider electrostatic inter-particle interactions, being only valid for neutral and spherical scattering centres, in dilute solutions; in other cases, it only provides an estimation of neutral-sphere-equivalent hydrodynamic diameters, Φ_e [29]. In this work, only the diffusion of pure DMPC liposomes (which are neutral and spherical) and cationic liposomes with low DTAC amounts are not significantly affected by inter-particle interactions.

Results and discussion

Electronic absorption

Figure 1 compares absorption spectra of Chl *a* dissolved in the organic solvent diethyl ether and incorporated in DMPC liposomes, DTAC pre-micelle and micelle media ($CMC \approx 22$ mM), and DMPC–DTAC vesicles and micelles. Except for diethyl ether, the original spectra presented background scattering (or turbidity) and were corrected using eq. 1: see the Experimental section and the Electronic Supplementary Information (ESI), Table S1. Table S2 (ESI) collects relevant spectral parameters of the Soret and Q bands of Chl *a*.

The distribution of solvent molecules (especially nucleophilic polar molecules) around the Mg (the metallic centre of chlorophyll) plays an important role in solvation and solvent-mediated Chl aggregation [42,43]. At ≈ 10 μ M, Chl *a* dissolves in diethyl ether in the monomeric form. The absorption spectrum (curve 1), with the Soret band more intense than the Q₁ band and good resolution of the four Q bands, is characteristic of the pigment in nucleophilic solvents with steric hindrance [42], such as diethyl ether. It indicates a 5-coordinated Mg, where the ligands are the four nitrogen atoms of the porphyrin macrocycle plus the oxygen of an ether molecule. This asymmetric coordination forces the macrocycle (responsible for the photophysical properties of the pigment) to be slightly non-planar, giving rise to the four, well-defined, Q bands.

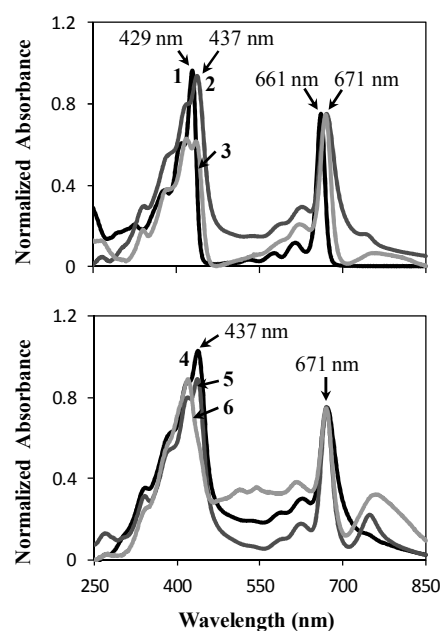


Figure 1. UV–visible absorption spectra of Chl *a* (normalized at the Q₁ band, after turbidity correction) in: 1, diethyl ether; 2, DMPC liposomes; 3, micelles (50 mM DTAC); 4, mixed liposomes at D:L = 1; 5, mixed micelles at D:L = 33; and 6, premicelle medium (5 mM DTAC).

In the DTAC–DMPC aqueous system (curves 2–6) the Chl *a* monomer spectra show poor resolution of the four Q bands. This low resolution is typical of Chl in nucleophilic solvents without steric hindrance [42], such as ethanol or water, with a 6-coordinated central Mg. Here, the two extra ligands (besides the four nitrogen atoms of the macrocycle) are the oxygens of two water molecules, placed at each side of the macrocycle, giving rise to a planar, more symmetric macro-cycle, and explaining the poorly-defined Q bands. The red shift of spectra 2–6 (10 ± 2 nm relatively to Chl in diethyl ether; see ESI, Table S2) agrees with this interpretation, i.e., it may be caused, in part, by a 6-coordinated Mg, which accepts electrons from the oxygens of the two water ligands [42]. This is a specific Chl–solvent interaction. Another origin for the red-shift is a general (bulk) solvent effect, caused by changes in the refractive index and dielectric constant, from the ether to the water medium [19].

Curve 6 (premicelle medium) presents extra bands near 500–550 nm, similarly to the pheophytin *a* spectrum [44]. Pheophytin is a Chl derivative without the central Mg, and usually originates as a degradation product of Chl in acidic media [45], which is not our case. In this premicelle medium, the bands near 500–550 nm appear well above the spectrum baseline because of huge background scattering (turbidity) of the sample; this means that the spectrum corresponds to large complexes of Chl *a* with DTAC, as also proved by FLIM data (see the FLIM images in ESI, Figure S4).

A longer wavelength band at ≈ 750 nm is also seen in all aqueous solutions. Red-shift absorption spectra of Chl *a* *in vivo* (P740, etc.), at very large Chl *a* concentrations ($\approx 10^{-1}$ M), generally results from aggregation or crystallization [46]. The

absorption spectrum, corresponding to the minute amount of Chl *a* soluble in water, shows an intense band at 745 nm that was ascribed to a strong excitonic coupling between the macrocycles, in aggregated forms [14]; and a less intense one at 670 nm. In our *in vitro* work, the ≈ 750 nm band coexists with ill-defined bands at ≈ 450 – 650 nm (seen in all aqueous solutions except in micelles); these bands can probably be attributed to unspecified (*unordered*) aggregates.

In DTAC micelles (curve **3**) the Soret band intensity no longer surpasses that of the Q_1 band. This feature is typical of Chl *a* in hydrogen-donor solvents, such as water, which can bond one hydrogen to the oxygen of ring V of the macrocycle [42]. Unexpectedly, this behavior was not systematically found in the other aqueous solutions studied, probably caused by the presence of residual diethyl ether (the delivery solvent for Chl).

Steady-state fluorescence

Figure 2 shows fluorescence emission spectra of Chl *a* in diethyl ether, DMPC liposomes, DTAC micelles, and DTAC–DMPC vesicles and micelles. J-type aggregates absorbing at ≈ 750 nm were found to be non-emissive, likely because they are partially or totally unordered.

In all aqueous media, the emission spectra of Chl *a* show the same λ_{max} , at 676 nm, red-shifted with respect to that in diethyl ether, at 663 nm. We attribute all aqueous spectra to the Chl *monomer*, because the red shift observed, ≈ 13 nm, is small and constant.

Comparing with ether, the emission of Chl *a* is quenched in DTAC–DMPC mixtures at low D:L ratios (Figure 2) and in pre-micelle media at low DTAC concentrations (ESI, Figure S1). This quenching is attributed to the formation of Chl *a* aggregates, which are formed in aqueous media in different proportions but are *much less emissive* than monomers (see the Fluorescence lifetimes and FLIM imaging subsections).

On the other hand, large DTAC amounts (in pure or mixed micelles) disrupt Chl–Chl interactions within aggregates; Chl monomers, with larger lifetimes, become dominant and bind to both types of micelles (see also the two next subsections).

Our results may be compared with those of Chl *a* interacting with thylakoid lipids. As an example, the influence of the lipid environment on the organization of the light-harvesting complex LHCII was studied at 77K by fluorescence spectroscopy [7]. It was found that addition of exogeneous thylakoid lipids (depending on their nature and concentration) to delipidated LHCII is able to modulate the spectroscopic properties of the LHCII aggregates, and thus regulate the thylakoid architecture and function: Whereas neutral galactolipids support the aggregated state of LHCII, anionic lipids exert a strong disaggregating effect on the complex. Our own data show that the *neutral* (zwitterionic) DMPC favors Chl *a* aggregation; this result is on the line with the data of ref. 7, with the reserve that different lipids were used in these two studies.

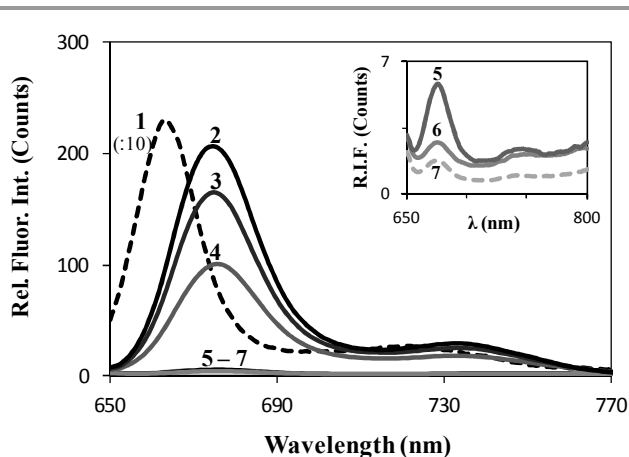


Figure 2. Emission spectra of Chl *a* in: diethyl ether (**1**); DTAC micelles (50 mM DTAC, **2**); DMPC–DTAC mixtures (**3–6**) with D:L = 33, 20, 4, and 2, respectively; and pure DMPC liposomes (**7**). The excitation was at 638 nm; the emission maxima are 663 nm (in ether) and 676 nm (in aqueous solutions). **Inset:** magnification of curves **5–7**.

Fluorescence lifetimes

Emission decays of Chl *a* in diethyl ether, DMPC liposomes, DTAC–DMPC mixtures, and DTAC micelles are illustrated in the ESI, Figure S2. The decays were fitted with a sum of exponential functions, eq. 2a, and the obtained pre-exponentials (amplitudes) and lifetimes are summarized in Table 1, together with the intensity-weighted average lifetimes, eqs. 2b,c, for a global comparison. Analogous information for Chl *a* in DTAC pre-micelle media is shown in the ESI, Figure S3 and Table S3.

Table 1. Pre-exponentials a and lifetimes τ , and average lifetimes τ_{av} , obtained from the analysis of Chl *a* fluorescence decays in DMPC liposomes, DTAC–DMPC vesicles and micelles, DTAC micelles, and diethyl ether. **V:** vesicles; **M:** micelles; **V/M:** coexistence of vesicles and micelles.

Solvent	a_1 /%	τ_1 /ns	a_2 /%	τ_2 /ns	a_3 /%	τ_3 /ns	τ_{av} /ns
DMPC vesicles	9	4.61	23	1.07	68	0.20	2.8
V, D:L = 0.3	11	4.96	19	1.12	70	0.15	3.4
V, D:L = 1.0	17	5.02	18	1.29	66	0.16	3.9
V, D:L = 2.0	5	4.54	13	1.03	82	0.14	2.5
V, D:L = 4.0	14	4.90	16	1.24	70	0.17	3.6
V, D:L = 6.7	7	5.36	5	0.96	88	0.09	4.1
V/M, D:L=12.5	7	5.35	5	0.92	88	0.09	4.1
M, D:L = 20	5	5.06	7	0.89	88	0.10	3.3
M, D:L = 33	23	5.14	12	1.40	65	0.09	4.5
DTAC micelles	80	5.32	20	1.64	—	—	5.1
Diethyl ether	100	5.80	—	—	—	—	5.8

In diethyl ether, a single exponential with a lifetime τ_1 of 5.8 ns fitted well the fluorescence decay of Chl *a*, in agreement with the *monomeric* state of the pigment. This value is in the same range of magnitude (≈ 5 to 6 ns) of reported lifetimes for monomeric Chl *a* isolated from different sources, in distinct organic solvents, e.g., 6.3 ns in methanol [47].

In DMPC liposomes and DTAC-DMPC vesicles and micelles, only 3-exponential functions could fit the Chl decays reasonably well, evidencing the coexistence of monomers and oligomers of the pigment: the longer component (≈ 5 ns) and minor population corresponds to the monomeric Chl *a*, and the two others (≈ 1 –2 and ≈ 0.1 –0.2 ns) to aggregates. Because higher order multi-exponential functions also fit the decays, aggregates possibly have *variable sizes and/or structures*. In DTAC-DMPC mixtures, monomer lifetimes, shorter than that in diethyl ether, tend to increase slightly with D:L. DMPC favors Chl aggregates, especially those with shorter lifetimes (70–90% population), at the expense of monomers.

Fast decay components, in the range of 2–3 ns, are usually found in *in vivo* systems. Average lifetimes of photosynthetic systems in the order of 0.7–2 ns were also obtained [48]. Similarly to our results in pure and mixed vesicles, a three-exponential function also fitted the fluorescence decay of Chl *a* in thylakoid membranes, with lifetimes of 4.55, 2.37, and 0.3 ns [49]. In this case, the intermediate lifetime had the highest fractional intensity (85%) in contrast with our data. Another example showed that the effect of aggregation of the complex LHCII on the decay kinetics of Chl *a* fluorescence could be accounted for by three exponential components [7]. Aggregation of LHCII led to fast deactivation of Chl *a* excited states; in this case, it is possible that both aggregation and structural changes of the LHCII protein will modify the spectral profile of Chl molecules and modulate their energy transfer and fluorescence kinetics [7]. In brief, the larger number of Chl molecules and their degree of organization in the living system contribute to increase the energy transfer efficiency, thus leading to shorter lifetimes than those usually found in *in vitro* systems.

In pure DTAC micelles, a bi-exponential function fitted the decays quite reasonably: monomers, with a lifetime τ_1 of 5.3 ns, are dominant (80%); and aggregates, with $\tau_2 = 1.6$ ns, are the minor population (20%). These data (conjugated with those obtained in the [FLIM Imaging](#) subsection) mean that DTAC micelles disaggregate most of Chl *a* oligomers and bind highly emissive monomers. A similar monomer lifetime, $\tau_1 = 5.01$ ns, was obtained for Chl *a* in nonionic Triton X-100 micelles, in conditions where all the Chl was monomeric [50].

FLIM imaging

FLIM was used to investigate both the *morphology* of colloidal microstructures and the *lifetimes* of the incorporated Chl *a* oligomers. [Figure 3](#) illustrates the emission intensity ([panel A](#)) and the normalized lifetime histogram ([C](#)) of the FLIM image ([B](#)) of Chl *a* in pure DMPC liposomes. Images were acquired directly in the aqueous solution deposited on the microscope coverslip, after giant (micro-sized) vesicles settled down.

Pure DMPC liposomes are very polydisperse ([Figure 3B](#)). The resolution of FLIM images only permits to observe the giant ones, in the micro-scale. Most vesicles are nearly spherical and *multilamellar* (MLVs, in *green–yellow*). A few unilamellar vesicles (ULVs, **1**) and vesicles inside other vesicles (**2**) also appear.

J-type Chl *a* aggregates, absorbing near 750 nm, cannot be excited herein — see the Experimental section, subsection Time-resolved fluorescence and fluorescence lifetime imaging microscopy (FLIM). It is also assumed that the phytol chain of Chl *a* (in monomers and/or aggregates) is inserted and oriented along the lipid chains, whereas the chlorin ring stays at the lipid/water interface [51].

In the *external* liposome bilayers, FLIM images showed a predominance of Chl monomers (in red) and few oligomers (*green–yellow*). Monomers are *highly emissive* and oligomers (*green–yellow*) are *strongly quenched* (see panel A, for the emission intensity). Oligomers are likely H-type dimers and/or larger aggregates. The fact that oligomers are still emissive indicates that they cannot be pure (totally ordered) H-aggregates. Lifetime distributions for Chl *a* (Panel C) show only one broad peak, meaning that populations of monomers and oligomers cannot be individualized; probably, several types/sizes of dimers/aggregates coexist.

In the *internal* bilayers, the green background means that most of the pigment is aggregated. H-type dimers might be easily formed possibly in an inter-bilayer fashion. However, formation of larger H-type aggregates cannot be excluded.

It is interesting to report (not shown herein) that Chl *a* lifetimes decrease along time: in freshly prepared liposomes, histograms are broadly centered at ≈ 4 ns; after one week, they peak at shorter lifetimes, ≈ 3 ns. These data mean that *Chl a aggregates are formed at slow rate* (in days), from monomers and/or smaller aggregates.

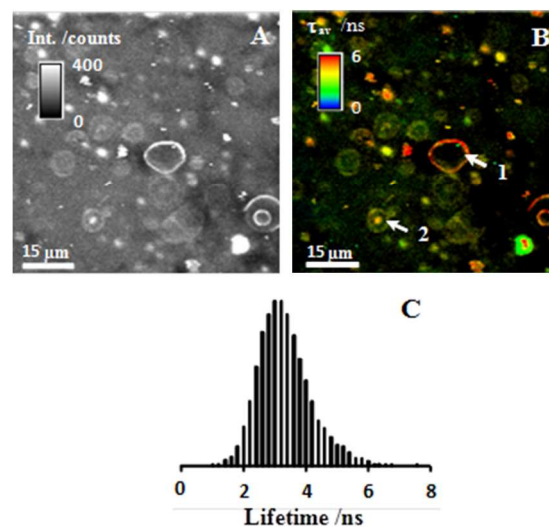


Figure 3. Emission intensity ([A](#)) and FLIM image ([B](#)) of Chl *a* in DMPC liposomes, measured in solution one week after preparation. The intensity and lifetime scales are shown at left. ([C](#)) Normalized Chl *a* lifetime histogram.

Figure 4 illustrates FLIM images of Chl *a* in mixed vesicles, at D:L = 1 (panel A) and 2 (C). In this D/L range, the liposome size decreases drastically as D:L increases. Vesicles with smaller diameters than the detection limit (≈ 320 nm) appear as fluorescent spots in the background, as if they were single molecules. The lifetime distribution profile of these images is broad and centered at ≈ 3 –4 ns (B, D), meaning that Chl monomers coexist with different types/sizes of aggregates.

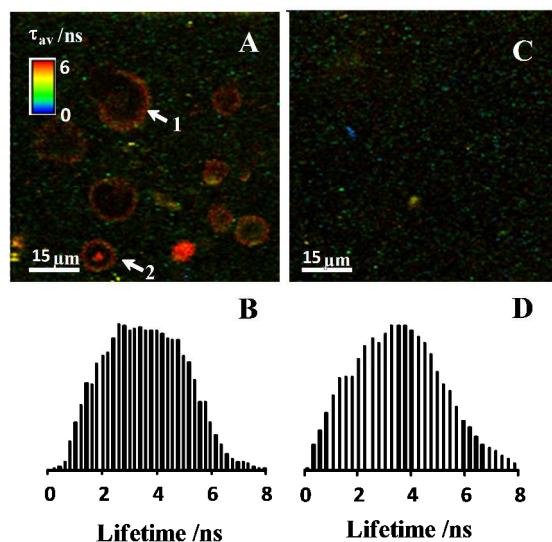


Figure 4. A,C: FLIM images of Chl *a* in the DTAC–DMPC mixed system, at D:L = 1 (A) and 2 (C). The lifetime scale is shown at left. B, D: Corresponding normalized Chl *a* lifetime histograms.

Giant vesicles are still observed at D:L = 1 (panel A). Some of them are *unilamellar* (e.g., 1), showing a black interior: the aqueous compartment devoid of Chl. Other vesicles are MLVs or contain smaller vesicles inside (2). Rupture of the bilayer is observed in vesicle 1, exposing its contents (water) to the exterior medium. Chl *a* monomers (red) are mainly distributed in the vesicles outer surfaces. Smaller vesicles containing Chl *a* aggregates are seen as green spots in the background.

At D:L = 2 (panel C), giant vesicles are practically absent and the size distribution becomes more homogeneous. A *green-bluish* spotted background means that Chl *a* aggregates largely predominate. Previous DLS data at this D:L showed that small ULVs (≈ 100 nm) coexist with even smaller disks (≈ 30 nm), both having low size polydispersity [29]. The single-chained DTAC forces a larger spontaneous curvature in vesicles (i.e., makes them smaller), thus acting as an “extruder”.

At D:L = 2–15, ULVs and disks coexist, with equivalent sizes remaining small and almost constant [29]. FLIM images taken in this D:L range were similar to Figure 4C (for D:L = 2), and are not shown herein.

Above D:L ≈ 15 , only mixed micelles exist [28]. Figure 5 shows FLIM images of Chl *a* in DTAC–DMPC micelles (A,C) and in pure DTAC micelles (E). As D:L increases (A→C→E), Chl *a* lifetimes shift to longer values (B→D→F), revealing the increasing dominance of pigment monomers.

At D:L = 15 (panel A), interesting elongated structures were visualized, previously proposed to be *cylindrical* (threadlike or wormlike) *micelles*, or *threads* [28,29]. Chl *a* aggregates (in green) are bound to these micelles. Colored background spots result from Chl *a* aggregates in mixed *spherical micelles*, which coexist with threads but are too small to be resolved by FLIM. The lifetimes distribution profile (panel B), peaked at ≈ 3.5 –4 ns, agree with the dominance of Chl aggregates in the sample.

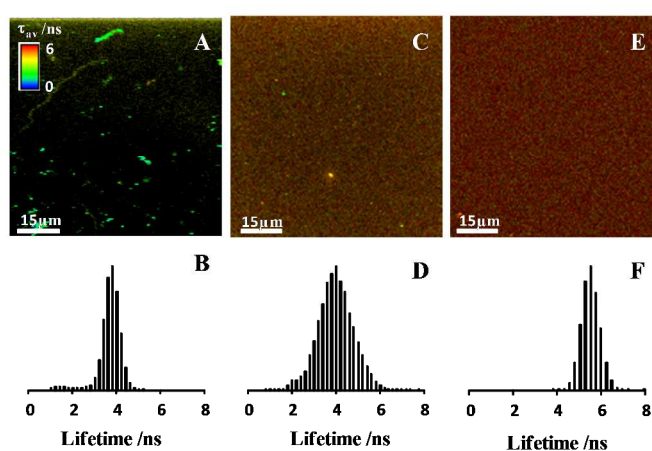


Figure 5. A,C,E: FLIM images of Chl *a* in the DTAC–DMPC mixed micelles at D:L = 15 (A) and 33 (C); and in DTAC micelles (50 mM DTAC; E). The lifetime scale is shown at left. B, D, F: Normalized Chl *a* lifetime histograms.

At D:L = 33 (Figure 5C), FLIM images are similar to those of pure DTAC (E), indicating that small *spherical micelles* become dominant. The *dense* background denotes a large concentration of micelles. The *brownish* background, with the lifetime distribution profile peaked at ≈ 4 ns (D), shows that, in mixed micelles, Chl *a* monomers still coexist with aggregates.

Finally, in pure DTAC micelles, both the *reddish* background (Figure 5E) and the lifetime distribution profile peaked at ≈ 5.5 ns (F) indicate the dominance of Chl *a* monomers. All these micelles are *spherical*: indeed, cryo-TEM micrographs of pure DTAC solutions were unable to detect threadlike micelles [52], even at 100 mM DTAC (more than 4 times the CMC).

FLIM results therefore corroborate those from fluorescence lifetime measurements (Table 1).

In pre-micelle media (5–15 mM DTAC), large, irregular, and heterogeneous microstructures appear (see ESI, Figure S5), which are probably Chl *a* unordered aggregates *complexed* with detergent DTA⁺ long ions.

FCS results

FCS measurements were performed for Chl *a* incorporated in pure DMPC liposomes, DTAC micelles, and DTAC–DMPC vesicles and micelles. Table S4 (in ESI) displays the fitted parameters of the diffusion model (calculated by eqs. 3 and 4); and the equivalent diameters (calculated by eq. 5) of the colloidal nanostructures, compared with those previously obtained by DLS measurements [29].

Figure 6 illustrates characteristic autocorrelation curves (1–5) and exemplifies typical size distributions (insets A, B, C).

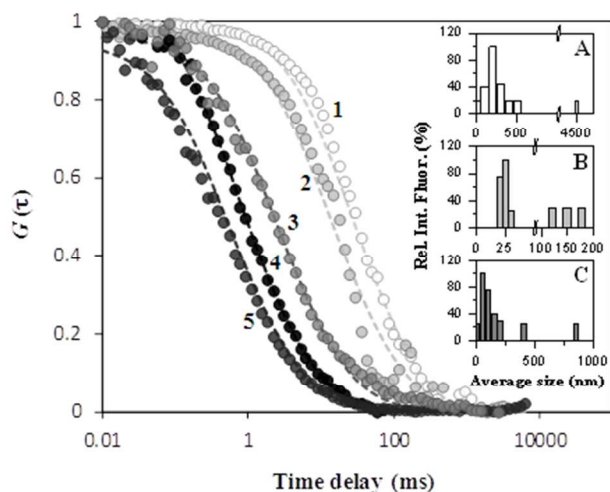


Figure 6. Typical normalized FCS autocorrelation curves for Chl *a* in: (1) pure DMPC liposomes; (2) mixed vesicles at D:L = 1; (3) disks, D:L = 4; (4) mixed spherical micelles, D:L = 33; and (5) pure DTAC micelles, 50 mM DTAC. **Insets:** Size distribution profiles for: (A) pure DMPC liposomes; (B) ULVs and disks, D:L = 4; and (C) spherical and threadlike micelles, D:L = 20.

Pure DMPC liposomes exhibit very large size polydispersity: diameters of 100–5000 nm were found (Figure 6, inset A). Spikes in the correlation curve (1) result from the sudden increase of the Chl fluorescence intensity, caused by the slow passage of large vesicles through the observation volume.

Spikes were also observed at D:L = 1 and 4 (curves 2 and 3). As a general trend, both the vesicle size and polydispersity decrease when increasing the DTAC amount (or the D/L ratio) in the mixtures, in agreement with the FLIM data.

At D:L = 4, two main populations, with low polydispersity, were obtained (Figure 6, inset B). The larger population still corresponds to ULVs (Φ_e centred at ≈ 150 nm) and the smaller one ($\Phi_e \approx 25$ nm) to disks [29]. Disks are likely formed from vesicle rupture and flattening of the resulting bilayer fragments: this rearrangement segregates the two components, the lipid at the central part of the disk; and the detergent at the rim, protecting the lipid hydrophobic chains from contact with water [52]. In the range of D:L ≈ 2 –10, micro-DSC has also revealed the coexistence of mixed liposomes and disks, the latter being smaller and more rigid than vesicles [28].

At D:L ≈ 15 –20 (inset C, for D:L = 20), small spherical micelles coexist with much larger structures, which, according to FLIM images (Figure 5A), were proposed to be threadlike micelles [28,29]. Values of neutral-sphere-equivalent diameters of threads ($\Phi_e \approx 80$ –700 nm) are only a rough, semi-quantitative estimation of their size. Threads, being very *slow-diffusing* and *slow-growing* [29] structures, have been frequently observed in detergent–phospholipid mixtures by cryo-TEM [53–55] and/or rheological measurements [55–57].

Spherical micelles always have small size polydispersities. In FCS measurements, mixed spherical micelles show larger equivalent hydrodynamic diameters (7.1 nm) than those obtained by DLS measurements (5.6 nm) [29]. This is caused by the incorporated Chl molecule, which significantly alters the size (and diffusion behavior) of these small micelles.

Finally, FCS measurements for (even smaller) pure DTAC micelles gave $\Phi_e = 4.6$ nm, also larger than a value reported in the literature in the absence of probes, 4.0 nm [58]. An even larger value of $\Phi_e = 5.5$ nm was retrieved using the probe tetrasulfonated aluminum phthalocyanine in DTAC micelles [59]; as compared to Chl, the larger, four negatively-charged, phthalocyanine macrocycle is attached to the DTA⁺ micelle surface by strong electrostatic attractions, without penetrating into the micelle, therefore further increasing the size of the diffusing entity. In other literature examples, incorporation of relatively bulky probes in micelles also led to determination of larger diameters than in the absence of probes [60,61].

Conclusions

The aggregation and disaggregation behavior of Chl *a*, inserted in spontaneous colloidal structures of the phospholipid DMPC and the detergent DTAC, was investigated using highly sensitive fluorescence techniques, mainly FLIM. FCS provided the mean size of vesicles, disks, and micelles.

Fluorescence decays and FLIM images showed a coexistence of Chl *a* monomers and oligomers in most colloidal structures. The aggregation states and fluorescence lifetimes of Chl were strongly affected by the architecture (or D:L molar ratio) of the colloidal media. Formation of aggregates (likely, H-type) of Chl *a* in vesicles inter-layers proves the dominance of Chl–Chl versus Chl–amphiphile interactions and produces partial fluorescence quenching. On the other hand, high DTAC amounts (in pure or mixed micelles) reform highly emissive Chl *a* monomers, indicating disruption of Chl–Chl interactions.

FCS colloidal nano-sizes agree with published DLS data [29]. Below D:L ≈ 2 , there is a transition from metastable MLVs of pure DMPC to spontaneous ULVs of DMPC–DTAC, of successively smaller size and polydispersity. ULVs and disks coexist at D:L ≈ 2 –10, showing constant equivalent hydrodynamic diameters and low size polydispersities. Bilayers are completely solubilized above D:L ≈ 15 –20, where large threadlike micelles coexist with small spherical micelles.

The results described herein for Chl *a* inserted in DMPC–DTAC (zwitterionic lipid – cationic detergent) vesicles and micelles contributed to a better understanding of the type of interactions present in these model systems of biomembranes.

Acknowledgements

The authors thank Professor Sílvia Costa for helpful comments. This work was supported by Projects POCL/PPCDT/QUI/58816/2004, REEQ/115/QUI/2005, and PEst-OE/QUI/UI0100/2011, funded by Fundação para a Ciência e a Tecnologia (FCT). R.F.C. acknowledges a PhD grant (SFRH/BD/41296/2007) from FCT.

References

- 1 A. Sholto and B. Ehrenberg, *Photochem. Photobiol. Sci.* 2008, **7**, 344.
- 2 H. Ibrahim, A. Kasselouri, C.J. You, P. Maillard, V. Rosilio, R. Pansu and P. Prognon, *J. Photochem. Photobiol. A: Chem.* 2011, **217**, 10.
- 3 M. Vermathen, M. Marzorati and P. Bigler, *J. Phys. Chem. B* 2013, **117**, 6990
- 4 W.-T. Li, H.-W. Tsao, Y.-Y. Chen, S.-W. Cheng and Y.-C. Hsu, *Photochem. Photobiol. Sci.* 2007, **6**, 1341.
- 5 I. Gomaa, S. E. Ali, T. A. El-Tayeb and M. H. Abdel-kader, *Photodiagnosis and Photodynamic Therapy* 2012, **9**, 362.
- 6 H. Kirchhoff, H. R. Hinz and J. Rosgen, *Biochim. Biophys. Acta* 2003, **1606**, 105.
- 7 S. Schaller, D. Latowski, M. Jemiola-Rzemińska, A. Dawood, C. Wilhelm and K. Strzalka, R. Goss, *Biochim. Biophys. Acta - Bioenergetics* 2011, **1807**, 326.
- 8 J. P. Markwell, J. P. Thornber and R. T. Boggs, *Proc. Natl. Acad. Sci. U.S.A.* 1979, **76**, 1233.
- 9 S. Santabarbara, K. V. Neverov, F. M. Garlaschi, G. Zucchelli and R. C. Jennings, *FEBS Letters* 2001, **491**, 109.
- 10 S. Santabarbara, R. Barbato, G. Zucchelli, F. M. Garlaschi, and R. C. Jennings, *FEBS Letters* 2001, **505**, 159.
- 11 S. Santabarbara, *Arch. Biochem. Biophys.* 2006, **455**, 77.
- 12 R. Vladkova, R. Koynova, K. Teuchner and B. Tenchov, *Biochim. Biophys. Acta - Biomembranes* 2010, **1798**, 1586.
- 13 L. L. Shipman, T. M. Cotton, J. R. Norris and J. J. Katz, *Proc. Natl. Acad. Sci. U.S.A.*, 1976, **93**, 1791.
- 14 J. J. Katz, L. L. Shipman, T. M. Cotton and T. J. Janson, in *The Porphyrins*, Academic Press, New York, 1978. Vol.5.
- 15 J. J. Katz, L. L. Shipman and J. R. Norris, in *Chlorophyll Organization and Energy Transfer in Photosynthesis*, Elsevier, Amsterdam, 1979.
- 16 J. J. Katz, M. K. Bowman, T. J. Michalski and D. L. Worcester, in H. Sheer (editor), *Chlorophylls*. CRC Press, Boca Raton, 1991, pp. 211-235.
- 17 A. Scherz, V. Rosenbach–Belkin and J. R. E. Ficher, in H. Sheer (editor), *Chlorophylls*. CRC Press, Boca Raton, 1991, pp. 237-268.
- 18 R. Vladkova, *Photochem. Photobiol.* 2000, **71**, 71.
- 19 A. Agostiano, P. Cosma, M. Trotta, L. Monsù-Scolaro and N. Micali, *J. Phys. Chem. B* 2002, **106**, 12820.
- 20 M. Tomkiewicz and G. A. Corker, *Photochem. Photobiol.* 1975, **22**, 249.
- 21 W. Oettmeier, J. R. Norris and J. J. Katz, *Biochem. Biophys. Res. Comm.* 1976, **71**, 445
- 22 H. Dijkmans, R. M. Leblanc, F. Cogniaux and J. Aghion, *Photochem. Photobiol.* 1979, **29**, 367.
- 23 J. H. Fendler, *J. Phys. Chem.* 1980, **84**, 1485
- 24 A. Agostiano, L. Catucci, G. Colafemmina and M. D. Monica, *Biophys. Chem.* 1996, **60**, 17.
- 25 M. X. Andersson and P. Dörman, in A. S. Sandelius and H. Aronsson (editors), *The Chloroplast: Interactions with the Environment*, Springer, Berlin, 2009.
- 26 M. S. Weeb and B. R. Green, *Biochim. Biophys. Acta* 1991, **1060**, 133.
- 27 N. Murata and N. Sato, *Plant Cell Physiol.* 1978, **19**, 401.
- 28 M. I. Viseu, R. F. Correia and A. C. Fernandes, *J. Colloid Interf. Sci.* 2010, **351**, 156.
- 29 R. F. Correia, M. I. Viseu, T. J. V. Prazeres and J. M. G. Martinho, *J. Colloid Interf. Sci.* 2012, **379**, 56.
- 30 K. Suhling, P. M. W. French and D. Phillips, *Photochem. Photobiol. Sci.* 2005, **4**, 13.
- 31 S. M. Andrade, R. Teixeira, S. M. B. Costa, A. J. F. N. Sobral, *Biophys. Chem.* 2008, **133**, 1.
- 32 M. I. Viseu, M. M. Velázquez, C. S. Campos, I. García-Mateos and S. M. B. Costa, *Langmuir* 2000, **16**, 4882.
- 33 M. I. Viseu, T. I. Carvalho, S. M. B. Costa, *Biophys. J.* 2004, **86**, 2392.
- 34 M. I. Viseu, A. S. Tatikolov, R. F. Correia, S. M. B. Costa, *J. Photochem. Photobiol. A: Chem.* 2014, **000**, 000 (accepted).
- 35 V. J. Klenin, *Thermodynamics of Systems Containing Flexible-Chain Polymers*. Elsevier, Amsterdam, 1999. Chapter 2.
- 36 B. Valeur, *Molecular Fluorescence: Principles and Applications*, 2001, Wiley-VCH verlag GmbH, chap. 6, p. 172.
- 37 S. M. Andrade, S. M. B. Costa, J. W. Borst, A. van Hoek, and A. J. W. G. Visser, *J. Fluoresc.* 2008, **18**, 601.
- 38 S. M. Andrade and S. M. B. Costa, *J. Photochem. Photobiol. A: Chem.* 2011, **217**, 125.
- 39 R. Rigler, Ü. Mets, J. Widengren and P. Kask, *Eur. Biophys. J.* 1993, **22**, 169.
- 40 E. Elson and D. Magde, *Biopolymers* 1974, **13**, 1.
- 41 U. Haupts, S. Maiti, P. Schuille and W. W. Webb, *Proc. Natl. Acad. Sci. U.S.A.* 1998, **95**, 13573.
- 42 I. Renge and R. Avarmaa, *Photochem. Photobiol.* 1985, **42**, 253.
- 43 K. Karki and D. Roccatano, *J. Chem. Theory Comput.* 2011, **7**, 1131.
- 44 O. Mass, M. Taniguchi, M. Ptaszek, J. W. Springer, K. M. Faries, J. R. Diers, D. F. Bocian, D. Holten and J. S. Lindsey, *New J. Chem.* 2011, **35**, 76.
- 45 C. Eijkelhoff and J.P. Dekker, *Photosynthesis Res.* 1999, **52**, 69.
- 46 K. Ballschmitter and J. J. Katz, *Nature* 1968, **220**, 1231.
- 47 D. M. Niedzwiedzki and R. E. Blakenship, *Photosynth. Res.* 2010, **106**, 227
- 48 V. Barzda, C. J. de Grauw, J. Vroom, F. J. Kleima, R. van Grondelle, H. van Amerongen and H. C. Gerritsen, *Biophys. J.* 2001, **81**, 538-546.
- 49 A. M. Gilmore, T. L. Hazlett and Govindjee, *Proc. Natl. Acad. Sci. U.S.A.* 1995, **92**, 2273.
- 50 M. I. Viseu and S. M. B. Costa, *J. Chem. Soc. Faraday Trans.* 1993, **89**, 1925.
- 51 J. Luisetti, H. Möhwald and H. J. Galla, *Biochemical and Biophysical Research Communications*, 1977, **78**, 754.
- 52 M. I. Viseu, K. Edwards, C. S. Campos and S. M. B. Costa, *Langmuir* 2000, **16**, 2105.
- 53 M. C. Sandström, E. Johansson and K. Edwards, *Langmuir* 2007, **23**, 4192.
- 54 E. Johansson, M. C. Sandstrom, M. Bergstrom and K. Edwards, *Langmuir* 2008, **24**, 1731.
- 55 L. Ziserman, L. Abezgauz, O. Ramon, S. R. Raghavan and D. Danino, *Langmuir* 2009, **25**, 10483.
- 56 S. R. Raghavan, G. Fritz and E. W. Kaler, *Langmuir* 2002, **18**, 3797.
- 57 D. Angelescu, A. Khan and H. Calderaru, *Langmuir* 2003, **19**, 9155.
- 58 B. L. Bales and R. Zana, *J. Phys. Chem. B* 2002, **106**, 1926.
- 59 R. F. Correia, S. M. Andrade, and M. I. Viseu, *J. Photochem. Photobiol. A: Chem.* 2012, **235**, 21.
- 60 M. A. Hink, A. Van Hoek and A. J. W. G. Visser, *Langmuir* 1999, **15**, 992.
- 61 M. Novo, S. Felekyan, C. A. M. Seidel and W. Al-Soufi, *J. Phys. Chem. B* 2007, **111**, 3614.